Ceramics International 45 (2019) 19331–19339

Contents lists available at ScienceDirect

Ceramics International

journal homepage: www.elsevier.com/locate/ceramint

Heat transfer, thermal stress and failure analyses in a TiB_2 gas turbine stator blade

Kourosh Vaferi[a], Sahar Nekahi[a], Mohammad Vajdi[a], Farhad Sadegh Moghanlou[a], Mohammadreza Shokouhimehr[b], Amir Motallebzadeh[c], Jianjun Sha[d], Mehdi Shahedi Asl[a,*]

[a] Department of Mechanical Engineering, University of Mohaghegh Ardabili, Ardabil, Iran
[b] Department of Materials Science and Engineering, Research Institute of Advanced Materials, Seoul National University, Seoul, 08826, Republic of Korea
[c] Koç University Surface Science and Technology Center (KUYTAM), Sariyer, Istanbul, 34450, Turkey
[d] State Key Laboratory of Structural Analysis for Industrial Equipment, Dalian University of Technology, Dalian, 116024, China

ARTICLE INFO

Keywords:
Titanium diboride
Principle stresses
Gas turbine blade
Brittle material
Coulomb–Mohr theory

ABSTRACT

Gas turbine stator blades do not experience centrifugal force contrary to the rotor blades; but they are exposed to high–temperature combustion gases causing thermal stresses. In the present work, a series of numerical simulations were carried out to clarify the feasibility of TiB_2 utilization as an appropriate material for gas turbine stator blades. The governing equations of heat transfer and solid mechanics were discretized by the finite element method and solved using Comsol Multiphysics software. The boundary conditions were applied, and temperature, displacement and maximum principle stress were obtained. The results showed that using ceramics such as TiB_2 instead of conventional alloys can enhance the maximum displacement. Temperature distribution in the blade is more uniform than that of alloys, and consequently, the thermal stresses are reduced. The TiB_2 can withstand the applied stresses according to the Coulomb–Mohr theory with a safety factor of 2.4.

1. Introduction

Turbines have broad application in thermal power generation units such as power plants (steam turbines and gas turbines), manufacturing and transportation systems. Gas turbines are common power generation plants and their flexibility to the fuels is one of the reasons for their extensive application in particular, renewable fuels *e.g.* biogas [1,2]. The turbine efficiency is in direct relation with working temperature and pressure ratio. Increasing the inlet gas temperature enhances the turbine efficiency considerably [3,4]. However, metallurgical limitations of the applied materials confine the turbine working temperatures. For eliminating these problems, two strategies are generally suggested: cooling of the blades, and selecting appropriate materials for manufacturing turbine parts, especially the blades [5]. The use of cooling ducts inside the blades are one of the common ways of protecting them against high temperatures. Nevertheless, cooling the blades, decreases the turbine efficiency. Therefore, new types of materials are needed to work at higher temperatures without any metallurgical problems [5]. It is also necessary to investigate the temperature distribution and consequent thermal stresses to evaluate the feasibility of the applied materials and cooling methods.

The previously conducted studies demonstrated significance of thermal stresses and temperature distribution in the turbine blades. Sadowski et al. [6] presented analytical methods for estimation of stresses in the turbine blade together with the solution to the problem. By using the Extended Finite Element Method (XFEM), the advanced damage was modeled numerically. They concluded that the critical threshold of the rotor speed with the turbine blade at the thin thermal barrier coating layer does not undergo damage by using the mentioned technique.

Mezur et al. [7] investigated the failure analysis in the first stage of blades of a 70 MW-gas turbine which made of Inconel 738LC (nickel-based alloy) after 24000 h of operation at high temperatures. They found out that high temperatures result in the transformation of MC to $M_{23}C_6$ carbide type at airfoil part of the blade. This transformation and carbide formation reduced the ductility of the alloy as its toughness and the lifetime consequently.

The study of the blade failures in gas turbine engines has been conducted by Hou et al. [8]. They pursued mechanical analyses and non-linear finite element method studies to determine the steady dynamic characteristics and stresses of blades. By evaluating these characteristics and stresses, they identified the reasons of blade failure. They reported that the thermal expansion, gas pressure, and centrifugal load at the stationary condition do not have a remarkable effect on crack

* Corresponding author.
E-mail address: shahedi@uma.ac.ir (M. Shahedi Asl).

https://doi.org/10.1016/j.ceramint.2019.06.184
Received 3 June 2019; Received in revised form 18 June 2019; Accepted 18 June 2019
Available online 19 June 2019

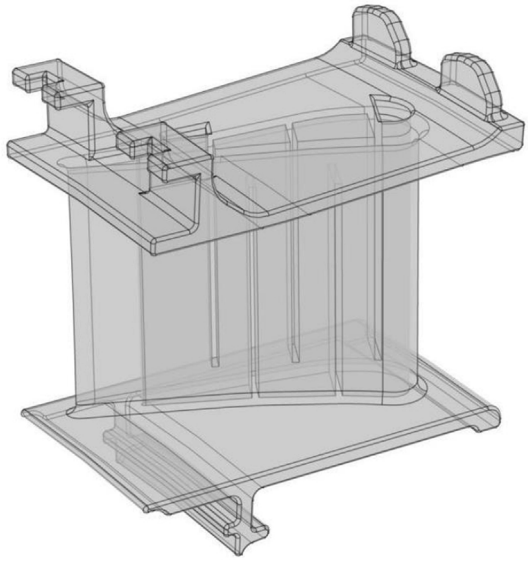

Fig. 1. The whole geometry of the turbine stator blade together with mounting details and cooling ducts.

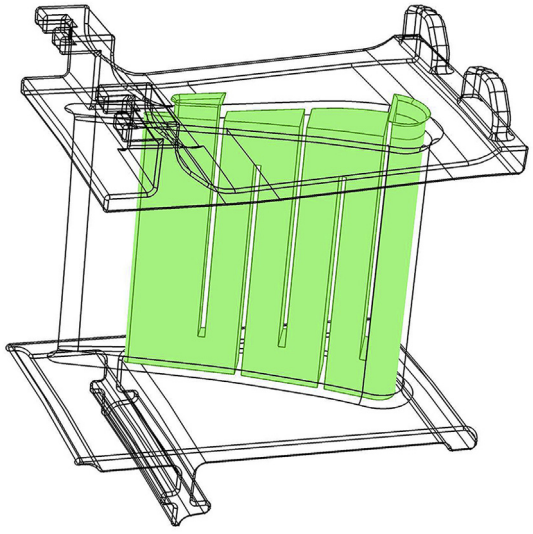

Fig. 2. Internal cooling ducts of blades.

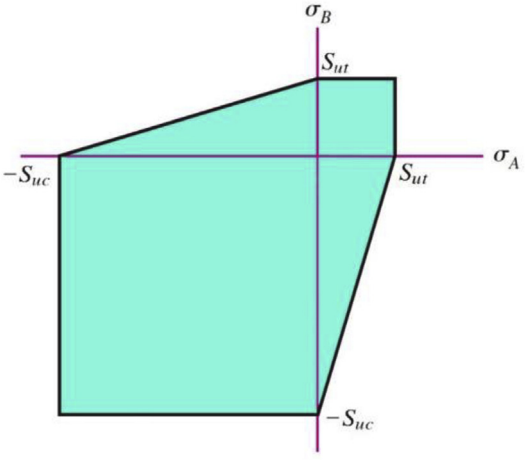

Fig. 3. The safety regions in Coulomb-Mohr theory.

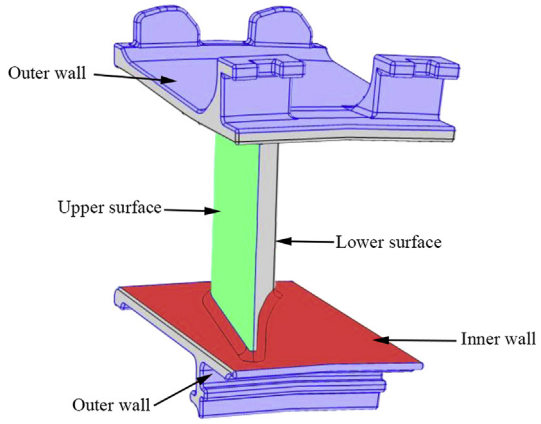

Fig. 4. The surfaces for applied thermal boundary conditions.

formation at the sharp leading corners.

Among the researches concentrating on the heat transfer of gas turbines studies, Kim et al. [9] rigorously examined the conjugation of convection and conduction heat transfer in the gas turbine as well as the weak points of hot parts of the turbine by obtaining the temperature distributions in a combustion liner. They reported that the heat transfer coefficients enhance sharply in the forward section.

Chyu et al. [10] investigated the heat transfer at the rectangular tip of the turbine blades. They stated that the influence of blade rotation on heat transfer is negligible. It should be noted that the study of heat transfer using several tip models, including flat and rectangular models, have been conducted in several papers [10–12]. They all concluded insignificant effect of relative motion on the tip heat transfer.

Nickel-based alloys, which have acceptable mechanical properties, are the common materials in producing turbine blades; however, at high temperatures, they encounter problems such as oxidation and creep caused deformations. In recent years, ceramic materials have been proposed for ultra-high temperature applications such as heat exchangers [13], and gas turbine blades [3]. The proposed ceramics can withstand higher temperatures with lower oxidation such as ZrB_2–SiC and HfB_2–SiC [14].

Ultra-high temperature ceramics (UHTC) are a group of materials with considerably high strength and melting point which offer good chemical and physical stabilities at high temperatures [15–24] which can be a proper candidate in the manufacturing of different parts of turbines.

ZrB_2, as a UHTC, has been proposed as a candidate for the manufacturing of gas turbine stator blade by our group [3,25–41]. They investigated a stator blade of gas turbine made of zirconium diboride and showed that ZrB_2 has a lower displacement in comparison with common metal-based blades. The more uniform temperature distribution was also reported [3]. Another diboride which has been used in many industrial applications is TiB_2. Titanium diboride as one of the UHTCs has very good mechanical and thermal properties such as high hardness (~32 GPa), high melting point (3225 °C), great elastic modulus (529 GPa) and excellent electrical and thermal conductivity (~10^5 S/cm and 60-120 w/m-k, respectively) [28,42–62], which makes it a promising candidate to adapt with harsh working environments like impact, corrosion, wear and high temperatures. TiB_2 has been used in various industries including manufacturing gas turbine blade materials, machine tools, engine valves, and ball bearings [52,55,62–64].

The main objective of the present research is to investigate the feasibility of using TiB_2 as turbine stator blade. TiB_2 can work at high operational temperatures, resulting in better power cycle efficiencies. In addition, the problems associated with metallurgical problems of commonly used alloys may be avoided. In this regard, a series of numerical simulations were carried out by the finite element method to

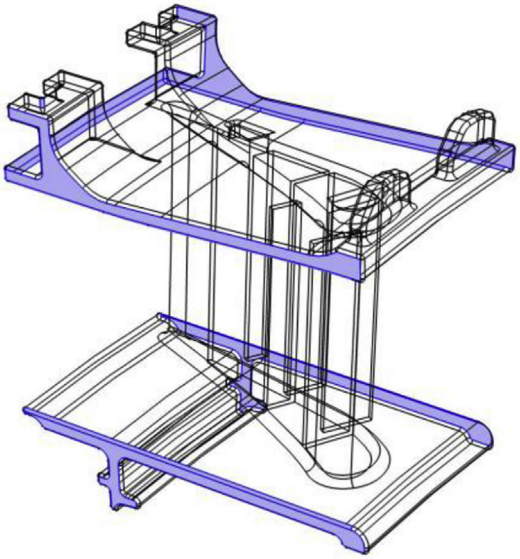

Fig. 5. Thermally insulated boundaries.

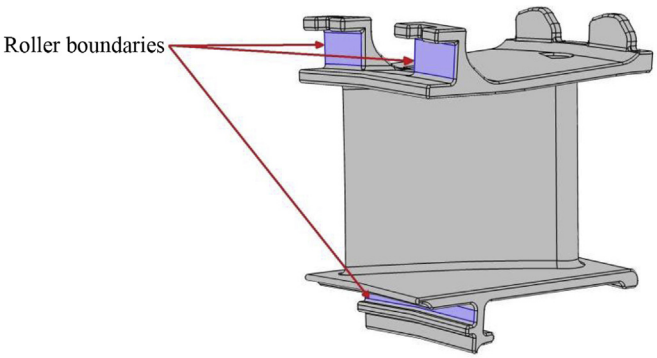

Fig. 6. The surfaces with roller boundary condition.

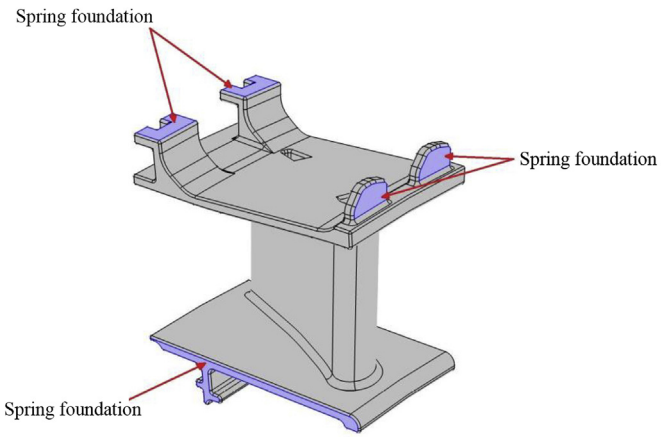

Fig. 7. The top view of spring foundations.

obtain the temperature distribution and resulted thermal stresses.

2. Methodology

2.1. Geometry

The geometry applied in the present work is a modified version of the selected geometry in Ref. [65]. The whole geometry of the turbine

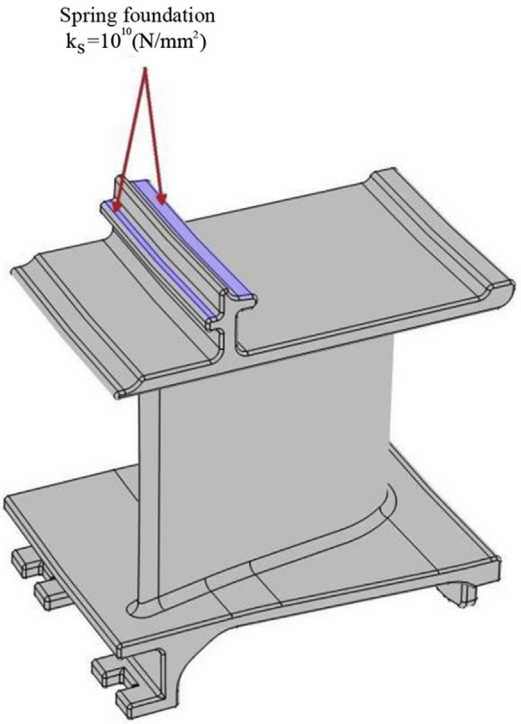

Fig. 8. The bottom view of boundary condition for spring foundation.

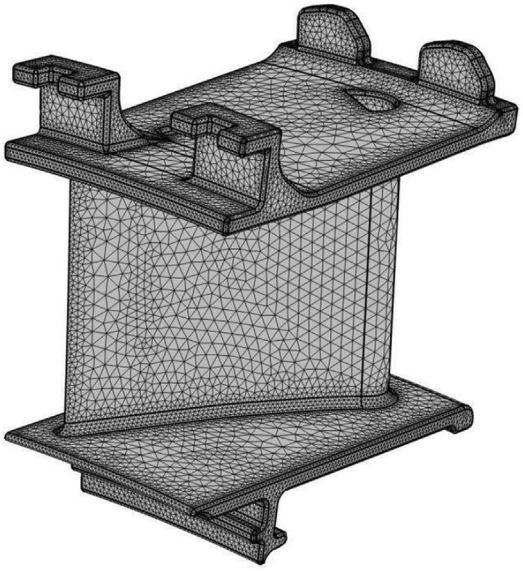

Fig. 9. The generated mesh on turbine stator blade.

stator blade together with mounting details and cooling ducts are presented in Fig. 1. At very high operating temperatures, the metallurgical problems such as corrosion, oxidation, and sulphidation are possible. Thus, for preventing these problems, the cooling of blades is essential. The air coming from the compressor passes among the internal ducts and cools the blades. Fig. 2 shows the internal cooling ducts of blades which have been used in the present work, however, for the convenience of calculation, the details of ribs geometry inside the ducts are neglected, and instead the average Nusselt number correlation is calculated for obtaining the heat transfer coefficient [3]. The air, as a cooling fluid, is considered at the pressure of 30 bar and the temperature of 600 K.

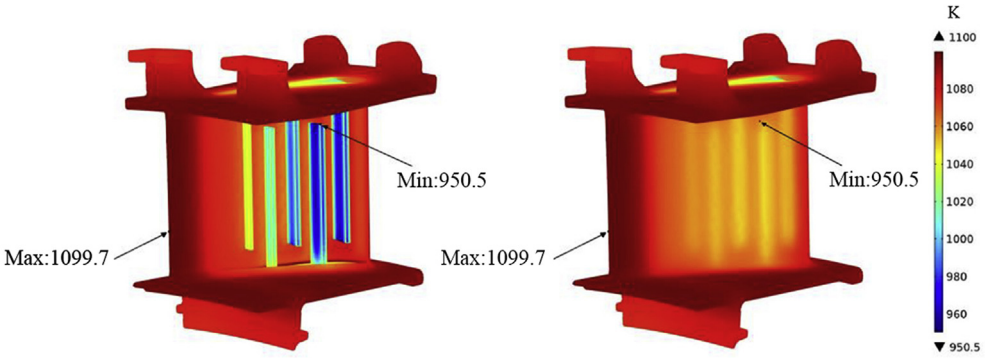

Fig. 10. The temperature distribution in the blade made of TiB_2 and cooling duct.

Table 1
The different temperatures of TiB_2, ZrB_2 ceramics and M152 alloy.

Average temperature (K)	Minimum temperature (K)	Maximum temperature (K)	Blade material
1070.1	867.8	1100.0	M152 alloy [3]
1079.1	953.9	1100.0	Zirconium diboride [3]
1078.9	950.5	1099.7	Titanium diboride

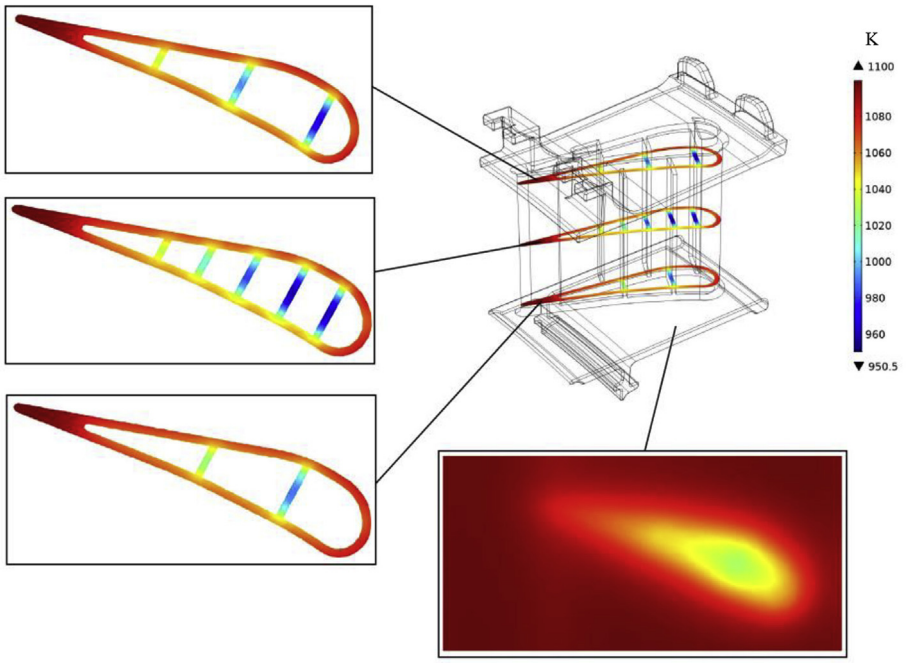

Fig. 11. 2D temperature contours in different sections of turbine blade.

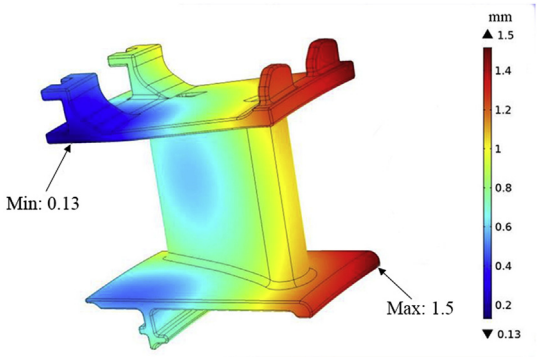

Fig. 12. The contours of displacement at various parts of the turbine blade.

2.2. Governing equations

The hot gases transfer the heat to the blade by convection mechanism while the transferred heat diffuses in the blade material by conduction. Temperature distribution through the blade results in thermal stresses due to the fixed supports. Therefore, two sets of governing equations are needed to cover both thermal behavior and mechanical characteristics of blades. The governing equations consist of heat diffusion and linear elastic equations. The heat diffusion equation is presented as Eq. (1) [3]:

$$\rho C\frac{\partial T}{\partial t} = \nabla.\,(k\nabla T) \tag{1}$$

where ρ, c and k are allocated to density, heat capacity and thermal conductivity of the blade material, respectively. The transferred heat

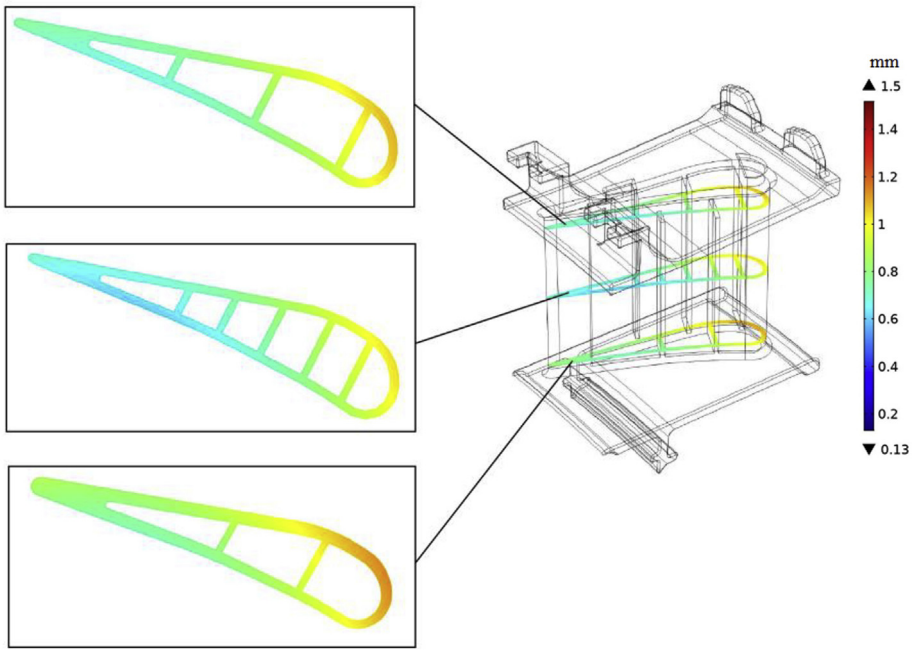

Fig. 13. The displacement of the blade at three different cross-sections.

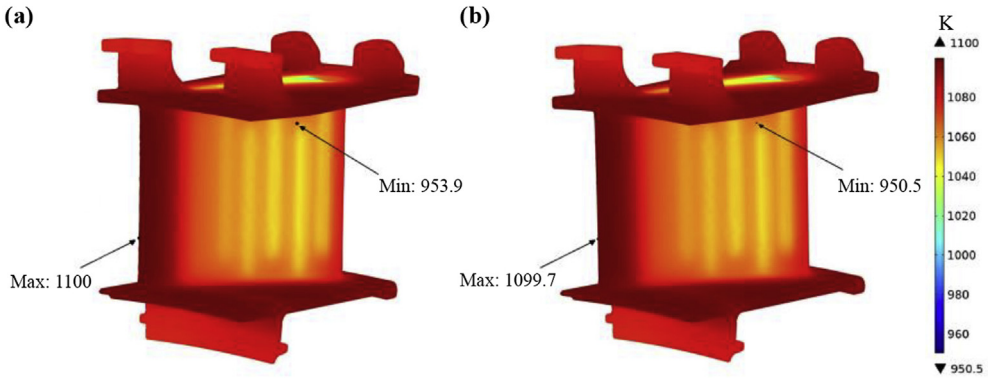

Fig. 14. The temperature distribution in the turbine blade made of (a) ZrB_2 [3] and (b) TiB_2.

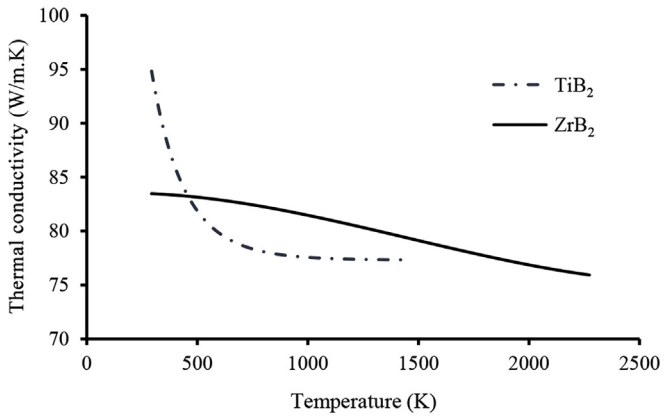

Fig. 15. Thermal conductivities of TiB_2 [42] and ZrB_2 [73].

from the surfaces in contact with the hot and cold fluid is obeying the Newton cooling law which is as:

$$q_0 = h(T_{ext} - T) \tag{2}$$

In which q_0 represent the heat flux and h is the convective heat transfer coefficient, T_{ext} and T represent the external fluid and the solid surface temperatures, respectively.

The general form of strain tensor for solid domain can be written as Eq. (3) [3]:

$$\varepsilon = \frac{\nabla\vec{u} + \nabla\vec{u}^T}{2} \tag{3}$$

where u shows the displacement vector. The relation between strain tensor, stress tensor and temperature is stated by Duhamel-Hook's law according to Eq. (4), in which D is elasticity tensor. In this relation, thermal expansion and other material properties are assumed to be isotropic and initial stresses and strains are neglected [3].

$$\sigma = D(\varepsilon - \alpha(T - T_0)) \tag{4}$$

In fact, D shows the stiffness matrix of materials and due to the symmetric condition it has, a 3×3 matrix indicates the three stress components [3].

$$\begin{bmatrix}\sigma_x\\ \sigma_y\\ \sigma_z\end{bmatrix} = \frac{E}{(1+\upsilon)(1-2\upsilon)}\begin{bmatrix}1-\upsilon & \upsilon & \upsilon\\ \upsilon & 1-\upsilon & \upsilon\\ \upsilon & \upsilon & 1-\upsilon\end{bmatrix}\begin{bmatrix}\varepsilon_x\\ \varepsilon_y\\ \varepsilon_z\end{bmatrix} \tag{5}$$

where σ, ε and υ are the stress, strain and the Poisson's ratio, respectively. E shows the Young's modulus. The linear relationship between

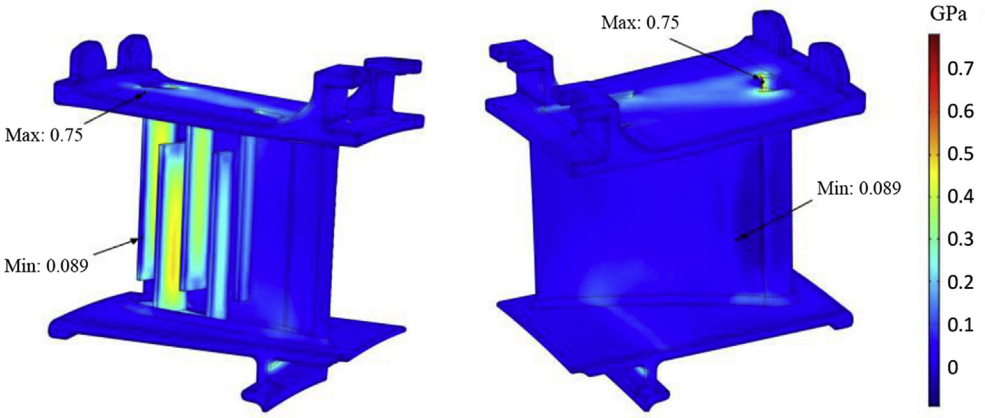

Fig. 16. The contour of principle compressive stresses.

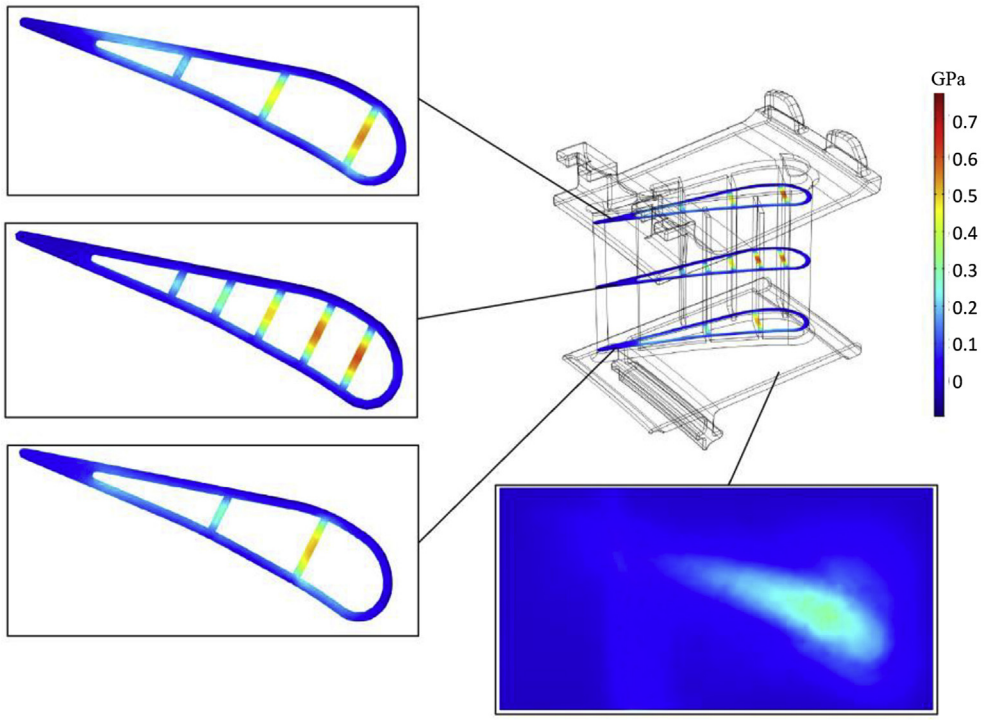

Fig. 17. The contour of principle compressive stresses in various cross sections.

strain and shear components is presented by Eq. (6). This relation is a function of Young's modulus and Poisson's ratio.

$$\tau_{ij} = \frac{E\varepsilon_{ij}}{(1-2\upsilon)} \tag{6}$$

The effective factors on rate of deformation are the properties of material, the applied load and the exposure temperature. In a number of cases such as ceramics, concretes, and other brittle materials the Coulomb-Mohr theory is a suitable criterion for investigating the probability of failure. If a component fails in a high speed gas turbine, the high rotational speed can lead to a full rupture of the whole turbine. The brittle materials have compressive strength more than their corresponding tensile values and TiB_2 as a ceramic material has brittle manner. The obtained stresses under the support forces and temperature gradients are the thermal stresses. Presence of the utilized supports as well as no possibility of movements for blade cause formation of compressive stresses when the body is heated and expanded [3]. Thermal stresses are dominant in this study which are compressive [3], so the third case of the Coulomb-Mohr theory is used for failure estimation of the blade made of TiB_2. The coulomb-Mohr theory can be formulated as Eq. (7):

$$\begin{aligned} &\sigma_A = \frac{S_{ut}}{n} && \sigma_A \geq \sigma_B \geq 0 \\ &\frac{\sigma_A}{S_{ut}} - \frac{\sigma_B}{S_{uc}} = \frac{1}{n} && \sigma_A \geq 0 \geq \sigma_B \\ &\sigma_B = -\frac{S_{uc}}{n} && 0 \geq \sigma_A \geq \sigma_B \end{aligned} \tag{7}$$

where n represents the factor of safety, σ_A and σ_B are the principle stresses, S_{ut} and S_{uc} are allocated to ultimate strength in tension and compression, respectively. The plot of Coulomb-Mohr failure theory is shown in Fig. 3. Any point in the colored area represents no failure condition.

2.3. Material properties

Despite rotor blades of the gas turbine, stator blades are stationary and no centrifugal force acts on them. So tensile stresses due to centrifugal force are neglected and most of the stresses generated in the

stator blades are due to fluid flow forces (drag and lift forces) and thermal stresses. The thermal stresses are dominant ones in the stator blades and are compressive. So ceramics are a good candidate because of their compressive strength. ZrB_2 with excellent mechanical properties [14,66–68] have been proposed and tested in the authors' previous paper [3] and the verification of the proposed numerical solution has been achieved. In this paper, monolithic TiB_2 as an UHTC with excellent mechanical and thermal properties is also chosen as the stator blade material and investigated numerically. The governing equations are solved by means of Comsol Multiphysics software. Comsol needs the mechanical and thermal properties of monolithic TiB_2 to solve the governing equations. The properties are obtained from the references [42,43] and presented as:

Elastic modulus (GPa):

$$E = E_0 + (dE/dT)(T - T_0) \tag{8}$$

where E_0 and T_0 are considered as 565 GPa and 296 K, respectively, for the temperature lower than 1000 °C, $dE/dT = -(0.032 \pm 0.015)$ GPa/K should be used.

Thermal conductivity (W/m.K):

$$k = 77.3 + \frac{8270 \times 10^{[-0.002\times(T-273)]}}{410 + (T - 273)} \tag{9}$$

Thermal diffusivity (m^2/s):

$$\alpha = 0.0000145 + \frac{0.00917 \times 10^{[-0.00279\times(T-273)]}}{530 + (T - 273)} \tag{10}$$

Specific heat capacity (J/kg.K):

$$C_p = 976 + 0.21 \times (T - 273) - 426 \times 10^{[-0.008\times(T-273)]} \tag{11}$$

The Poisson's ratio is considered as 0.111 based on Refs. [42,69].

2.4. Boundary conditions

The surfaces which were used as places of thermal boundaries are demonstrated in Fig. 4. The heat flux on the blade surfaces is determined using the convective heat transfer coefficient. In this regard, the pressure and suction sides are approximated as two flat plates employing the local heat transfer coefficient for external forced convection. The coefficient of convective heat transfer is given by Eq. (12), in which x is distance from the starting point of the plate and the parameter of U, which is used in the Reynolds number relation, is the fluid flow velocity. The allocated values of velocity for upper surface (suction side), the lower surface (stator pressure side) and the alongside platform walls are 300, 450 and 350 m/s, respectively [3,70]. The temperature of air (combustion gases) is 1100 k as well as a pressure of 30 bar, and the evaluated temperature of materials data is $(T_{surface} + T_{gas})/2$. The working temperature of turbine is considered at 900 K and the coefficient of heat transfer is 25 W/m^2.K. It is worth noting that the sound speed is about 650 m/s, and following that the Mach number is approximately 0.7 for concave side and 0.45 for convex sides which means that the flow is subsonic and the convective heat transfer coefficients can be calculated by Eq. (12) [71].

$$h = \frac{k}{x} pr^{\frac{1}{3}} \times \begin{cases} 0.332\,\mathrm{Re}_x^{\frac{1}{2}} & \mathrm{Re}_x \leq 5 \times 10^5 \\ 0.0296\,\mathrm{Re}_x^{\frac{4}{5}} & \mathrm{Re}_x \geq 5 \times 10^5 \end{cases} \tag{12}$$

In the present work, for simplifying the simulation of flow in ducts, the average Nusselt number of 400 was considered for cooling ducts and the related heat flux was calculated by Ref. [3]:

$$q'' = \frac{Nu_{cool}\mu_{cool}C_{cool}}{2Pr_{cool}H_{cool}}(T_{cool} - T) \tag{13}$$

where μ, C and H represented the viscosity of cooling air, specific heat capacity and the characteristic length of cooling ducts, respectively. The rest boundary conditions, shown in Fig. 5, are considered thermally insulated.

The roller and spring foundation was used as coupling of the stator parts to the supports. The rest of the boundaries are free to deform because of thermal expansion. The roller boundary conditions is indicated in Fig. 6, in which the body only allowed to move in parallel direction to specified surface which obeys the following relation:

$$u.\,n = 0 \tag{14}$$

where n is surface normal vector. The movement of top and bottom surfaces of stator blade is controlled by spring foundation which its boundary condition is given by Eq. (15) and shown in Figs. 7 and 8. K_s is allocated to the stiffness of spring foundation while F and u are the applied forces and displacement, respectively.

$$F = -K_s(u - u_0) \tag{15}$$

The meshed geometry is displayed in Fig. 9. In order to obtain results independent of mesh, different size of unstructured tetrahedral elements were generated and mesh independency was obtained by 147481 elements.

3. Results and discussion

A numerical heat transfer and thermal stress analysis were carried out to investigate the feasibility of using Titanium diboride as turbine stator blade material. At first, the described numerical method verified by the authors' previous paper [3] with the same geometry, material and boundary conditions. Then, the simulations were developed for TiB_2. The temperature distribution in blades and the cooling ducts is presented in Fig. 10 which helps better understanding of cooling effect. As it can be seen, the minimum temperature of 950.5 K arises at the cooling duct. On the other hand, the maximum temperature of 1099.7 K arises at the trailing edge and after that at the mounting parts which are located at the farthest distance from the internal cooling duct. It can be concluded that internal cooling has a significant influence on cooling process of blades. The maximum and minimum temperatures of blades made of different materials are presented in Table 1. Comparing to Ref. [3] the maximum temperature is almost the same, because the thermal resistance in the blade to blade passage is the same and is not a function of the blade material, while the minimum temperature is reduced in comparison with a blade ZrB_2 but increased comparing to the M152 alloy.

As a result of internal cooling, the temperature distribution is not uniform. The differences in temperature distribution are the main reason for the formation of thermal stresses. The trailing edge reaches a very high temperature approximately close to the temperature of combustion gases which may be because of insufficient cooling or higher convection coefficient of the high–speed combustion gases. The higher temperature gradient may lead to cracks formation and propagation near the internal cooling ducts and may result in blade failure. Fig. 11 shows the two-dimensional contours of temperature in different sections of the turbine blade.

Fig. 12 demonstrates the contours of displacement at various parts of the turbine blade made of TiB_2. The minimum displacement of 0.13 mm occur in thermal insulation wall, and the maximum displacement of 1.5 mm occur in the upper wall. As shown in Fig. 12, the displacement is reduced from the leading edge of the blade to the trailing edge due to the roller and spring supports, respectively. The leading edge is near the internal cooling duct that causes higher temperature difference, and because of this thermal gradient, the leading edge has more displacement than trailing edge [72]. Compared to ZrB_2, the maximum displacement is more than that of TiB_2, which is a result of higher thermal expansion of TiB_2. The displacement of different cross–sections of the blade is also shown in Fig. 13.

For comparing the results of temperature distribution in ZrB_2 ceramic and TiB_2 as the alternative material, Fig. 14 is presented. Based

on obtained contours, TiB_2 possesses the more temperature difference in the surface of the blade while temperature distribution in a blade made of ZrB_2 is more uniform. Referring to Table 1, the difference between maximum and minimum temperatures is higher for TiB_2 compared to ZrB_2, and it is worth noting that the higher temperature difference in the blade made of TiB_2 causes higher thermal gradient and results in higher thermal stresses in turbine blades. The changes in thermal conductivities versus temperature for TiB_2 and ZrB_2 materials are given in Fig. 15. The thermal conductivity of TiB_2 drops sharply at temperatures lower than about 800 K, and in the temperature range between 800-1400 K, the TiB_2 ceramic has the thermal conductivity coefficient lower than ZrB_2 and this is the reason of more non-uniform distribution of temperature in turbine blade made of TiB_2.

Since TiB_2 is classified as a brittle material, Coulomb–Mohr theory is the most appropriate one to estimate the probability of the blade failure. In this regard, maximum compressive principle stress is used along with the third case of the Coulomb-Mohr theory. In Fig. 16, the maximum compressive principle stress in the turbine blade is shown. The maximum compressive stress of 0.75 GPa is obtained at the internal cooling duct, which is not more than the reported value of 1.8 GPa for ultimate compression strength S_{uc} [42]. It seems that the gas turbine blade made of TiB_2 can withstand the compressive stresses and does not fail with the safety factor of 2.4. Besides, the minimum stress 0.089 GPa is observed near the tip of the turbine blade and indicates that the minimum possibility of failure occurs in these regions. Fig. 17 demonstrates the details of principle stresses in different cross sections of the turbine.

4. Conclusions

In the present study, TiB_2 is selected as an alternative material in manufacturing gas turbine stator blades, and the thermal stresses and temperature distribution is calculated. The paper has presented a numerical solution to investigate heat transfer in turbine stator blades and obtain the thermal stresses via Comsol Multiphysics software. The authors have also considered the consequences of deformation and the possibility of failure as a result of thermal compression stresses. The obtained results were broadly consistent with the reported data of ZrB_2 with the same geometry and applied boundary conditions. The results show that the high thermal conductivity of TiB_2 leads to a faster heat transfer in this ceramic as well as a reduction in thermal stresses. On the other hand, according to Coulomb-Mohr theory, the calculated safety factor ($n = 2.4$) is more than unity and states that the turbine can withstand the applied compressive loads due to high temperatures does not fail. Compared to the ZrB_2, TiB_2 experiences more maximum displacement.

References

[1] T. Gholizadeh, M. Vajdi, F. Mohammadkhani, Thermodynamic and thermo-economic analysis of basic and modified power generation systems fueled by biogas, Energy Convers. Manag. 181 (2019) 463–475, https://doi.org/10.1016/j.enconman.2018.12.011.

[2] T. Gholizadeh, M. Vajdi, H. Rostamzadeh, Energy and exergy evaluation of a new bi-evaporator electricity/cooling cogeneration system fueled by biogas, J. Clean. Prod. (2019), https://doi.org/10.1016/j.jclepro.2019.06.086.

[3] F. Sadegh Moghanlou, M. Vajdi, A. Motallebzadeh, J. Sha, M. Shokouhimehr, M. Shahedi Asl, Numerical analyses of heat transfer and thermal stress in a ZrB2 gas turbine stator blade, Ceram. Int. (2019), https://doi.org/10.1016/j.ceramint.2019.05.344.

[4] R.E. Sonntag, C. Borgnakke, G.J. Van Wylen, S. Van Wyk, Fundamentals of Thermodynamics 6 Wiley, New York, 1998.

[5] W.R. Martens, W.A. Raabe, The materials challenge of high-temperature turbine vanes and blades, ASME 1967 Gas Turbine Conf. Prod. Show, ASME, 1967, , https://doi.org/10.1115/67-GT-17 p. V001T01A017.

[6] T. Sadowski, P. Golewski, Detection and numerical analysis of the most efforted places in turbine blades under real working conditions, Comput. Mater. Sci. 64 (2012) 285–288, https://doi.org/10.1016/j.commatsci.2012.02.048.

[7] Z. Mazur, A. Luna-Ramírez, J.A. Juárez-Islas, A. Campos-Amezcua, Failure analysis of a gas turbine blade made of Inconel 738LC alloy, Eng. Fail. Anal. 12 (2005) 474–486, https://doi.org/10.1016/j.engfailanal.2004.10.002.

[8] J. Hou, B.J. Wicks, R.A. Antoniou, An investigation of fatigue failures of turbine blades in a gas turbine engine by mechanical analysis, Eng. Fail. Anal. 9 (2002) 201–211, https://doi.org/10.1016/S1350-6307(01)00005-X.

[9] K.M. Kim, N. Yun, Y.H. Jeon, D.H. Lee, H.H. Cho, S.-H. Kang, Conjugated heat transfer and temperature distributions in a gas turbine combustion liner under base-load operation, J. Mech. Sci. Technol. 24 (2010) 1939–1946, https://doi.org/10.1007/s12206-010-0625-8.

[10] M.K. Chyu, H.K. Moon, D.E. Metzger, Heat transfer in the tip region of grooved turbine blades, J. Turbomach. 111 (1989) 131, https://doi.org/10.1115/1.3262247.

[11] D.E. Metzger, R.S. Bunker, M.K. Chyu, Cavity heat transfer on a transverse grooved wall in a narrow flow channel, J. Heat Transf. 111 (1989) 73, https://doi.org/10.1115/1.3250661.

[12] J.S. Kwak, J.-C. Han, Heat transfer coefficients and film-cooling effectiveness on a gas turbine blade tip, J. Heat Transf. 125 (2003) 494, https://doi.org/10.1115/1.1565096.

[13] S. Nekahi, M. Vajdi, F.S. Moghanlou, K. Vaferi, A. Motallebzadeh, M. Ozen, U. Aydemir, J. Sha, M. Shahedi Asl, TiB2–SiC-based ceramics as alternative efficient micro heat exchangers, Ceram. Int. (2019), https://doi.org/10.1016/j.ceramint.2019.06.150.

[14] R. Tandon, H.P. Dumm, E.L. Corral, R.E. Loehman, P.G. Kotula, Ultra High Temperature Ceramics for Hypersonic Vehicle applications., Albuquerque, NM, and Livermore, CA, (2006), https://doi.org/10.2172/887260.

[15] W.G. Fahrenholtz, G.E. Hilmas, I.G. Talmy, J.A. Zaykoski, Refractory diborides of zirconium and hafnium, J. Am. Ceram. Soc. 90 (2007) 1347–1364, https://doi.org/10.1111/j.1551-2916.2007.01583.x.

[16] S. Zhu, W.G. Fahrenholtz, G.E. Hilmas, Influence of silicon carbide particle size on the microstructure and mechanical properties of zirconium diboride–silicon carbide ceramics, J. Eur. Ceram. Soc. 27 (2007) 2077–2083, https://doi.org/10.1016/j.jeurceramsoc.2006.07.003.

[17] Z. Balak, M. Azizieh, H. Kafashan, M. Shahedi Asl, Z. Ahmadi, Optimization of effective parameters on thermal shock resistance of ZrB2-SiC-based composites prepared by SPS: using Taguchi design, Mater. Chem. Phys. 196 (2017) 333–340, https://doi.org/10.1016/j.matchemphys.2017.04.062.

[18] Z. Balak, M. Shahedi Asl, M. Azizieh, H. Kafashan, R. Hayati, Effect of different additives and open porosity on fracture toughness of ZrB2–SiC-based composites prepared by SPS, Ceram. Int. 43 (2017) 2209–2220, https://doi.org/10.1016/j.ceramint.2016.11.005.

[19] M. Shahedi Asl, M. Ghassemi Kakroudi, Characterization of hot-pressed graphene reinforced ZrB2–SiC composite, Mater. Sci. Eng. A 625 (2015) 385–392, https://doi.org/10.1016/j.msea.2014.12.028.

[20] M. Shahedi Asl, M. Ghassemi Kakroudi, R. Abedi Kondolaji, H. Nasiri, Influence of graphite nano-flakes on densification and mechanical properties of hot-pressed ZrB2–SiC composite, Ceram. Int. 41 (2015) 5843–5851, https://doi.org/10.1016/j.ceramint.2015.01.014.

[21] Z. Ahmadi, B. Nayebi, M. Shahedi Asl, M. Ghassemi Kakroudi, Fractographical characterization of hot pressed and pressureless sintered AlN-doped ZrB2–SiC composites, Mater. Char. 110 (2015) 77–85, https://doi.org/10.1016/j.matchar.2015.10.016.

[22] M. Shahedi Asl, B. Nayebi, Z. Ahmadi, P. Pirmohammadi, M. Ghassemi Kakroudi, Fractographical characterization of hot pressed and pressureless sintered SiAlON-doped ZrB2–SiC composites, Mater. Char. 102 (2015) 137–145, https://doi.org/10.1016/j.matchar.2015.03.002.

[23] M. Shahedi Asl, M. Ghassemi Kakroudi, S. Noori, Hardness and toughness of hot pressed ZrB2–SiC composites consolidated under relatively low pressure, J. Alloy. Comp. 619 (2015) 481–487, https://doi.org/10.1016/j.jallcom.2014.09.006.

[24] M. Shahedi Asl, M. Ghassemi Kakroudi, B. Nayebi, H. Nasiri, Taguchi analysis on the effect of hot pressing parameters on density and hardness of zirconium diboride, Int. J. Refract. Metals Hard Mater. 50 (2015) 313–320, https://doi.org/10.1016/j.ijrmhm.2014.09.006.

[25] M. Shahedi Asl, B. Nayebi, M.G. Kakroudi, M. Shokouhimehr, Investigation of hot pressed ZrB2–SiC–carbon black nanocomposite by scanning and transmission electron microscopy, Ceram. Int. (2019), https://doi.org/10.1016/j.ceramint.2019.05.211.

[26] M. Shahedi Asl, B. Nayebi, M. Shokouhimehr, TEM characterization of spark plasma sintered ZrB 2 –SiC–graphene nanocomposite, Ceram. Int. 44 (2018) 15269–15273, https://doi.org/10.1016/j.ceramint.2018.05.170.

[27] S. Parvizi, Z. Ahmadi, M.J. Zamharir, M. Shahedi Asl, Synergistic effects of graphite nano-flakes and submicron SiC particles on the characteristics of spark plasma sintered ZrB2 nanocomposites, Int. J. Refract. Metals Hard Mater. 75 (2018) 10–17, https://doi.org/10.1016/j.ijrmhm.2018.03.017.

[28] M. Shahedi Asl, B. Nayebi, Z. Ahmadi, M. Jaberi Zamharir, M. Shokouhimehr, Effects of carbon additives on the properties of ZrB2–based composites: a review, Ceram. Int. 44 (2018) 7334–7348, https://doi.org/10.1016/j.ceramint.2018.01.214.

[29] M. Shahedi Asl, A statistical approach towards processing optimization of ZrB2–SiC–graphite nanocomposites. Part I: relative density, Ceram. Int. 44 (2018) 6935–6939, https://doi.org/10.1016/j.ceramint.2018.01.122.

[30] M. Shahedi Asl, M.J. Zamharir, Z. Ahmadi, S. Parvizi, Effects of nano-graphite content on the characteristics of spark plasma sintered ZrB2–SiC composites, Mater. Sci. Eng. A 716 (2018) 99–106, https://doi.org/10.1016/j.msea.2018.01.038.

[31] M. Shahedi Asl, Microstructure, hardness and fracture toughness of spark plasma sintered ZrB2–SiC–Cf composites, Ceram. Int. 43 (2017) 15047–15052, https://doi.org/10.1016/j.ceramint.2017.08.030.

[32] I. Farahbakhsh, Z. Ahmadi, M. Shahedi Asl, Densification, microstructure and mechanical properties of hot pressed ZrB2–SiC ceramic doped with nano-sized carbon

black, Ceram. Int. 43 (2017) 8411–8417, https://doi.org/10.1016/j.ceramint.2017.03.188.
[33] Z. Ahmadi, B. Nayebi, M. Shahedi Asl, M. Ghassemi Kakroudi, I. Farahbakhsh, Sintering behavior of ZrB2–SiC composites doped with Si3N4: a fractographical approach, Ceram. Int. 43 (2017) 9699–9708, https://doi.org/10.1016/j.ceramint.2017.04.144.
[34] Y. Orooji, M.R. Derakhshandeh, E. Ghasali, M. Alizadeh, M. Shahedi Asl, T. Ebadzadeh, Effects of ZrB2 reinforcement on microstructure and mechanical properties of a spark plasma sintered mullite-CNT composite, Ceram. Int. (2019), https://doi.org/10.1016/j.ceramint.2019.05.113.
[35] M. Khoeini, A. Nemati, M. Zakeri, M. Shahedi Asl, Pressureless sintering of ZrB2 ceramics codoped with TiC and graphite, Int. J. Refract. Metals Hard Mater. 81 (2019) 189–195, https://doi.org/10.1016/j.ijrmhm.2019.02.026.
[36] B. Mohammadpour, Z. Ahmadi, M. Shokouhimehr, M. Shahedi Asl, Spark plasma sintering of Al-doped ZrB2–SiC composite, Ceram. Int. 45 (2019) 4262–4267, https://doi.org/10.1016/j.ceramint.2018.11.098.
[37] A. Sabahi Namini, Z. Ahmadi, A. Babapoor, M. Shokouhimehr, M. Shahedi Asl, Microstructure and thermomechanical characteristics of spark plasma sintered TiC ceramics doped with nano-sized WC, Ceram. Int. 45 (2019) 2153–2160, https://doi.org/10.1016/j.ceramint.2018.10.125.
[38] A. Babapoor, M.S. Asl, Z. Ahmadi, A.S. Namini, Effects of spark plasma sintering temperature on densification, hardness and thermal conductivity of titanium carbide, Ceram. Int. 44 (2018) 14541–14546, https://doi.org/10.1016/j.ceramint.2018.05.071.
[39] Y. Azizian-Kalandaragh, A.S. Namini, Z. Ahmadi, M. Shahedi Asl, Reinforcing effects of SiC whiskers and carbon nanoparticles in spark plasma sintered ZrB2 matrix composites, Ceram. Int. 44 (2018) 19932–19938, https://doi.org/10.1016/j.ceramint.2018.07.258.
[40] E. Ghasali, M. Shahedi Asl, Microstructural development during spark plasma sintering of ZrB2–SiC–Ti composite, Ceram. Int. 44 (2018) 18078–18083, https://doi.org/10.1016/j.ceramint.2018.07.011.
[41] M. Shahedi Asl, B. Nayebi, Z. Ahmadi, S. Parvizi, M. Shokouhimehr, A novel ZrB2–VB2–ZrC composite fabricated by reactive spark plasma sintering, Mater. Sci. Eng. A 731 (2018) 131–139, https://doi.org/10.1016/j.msea.2018.06.008.
[42] R.G. Munro, Material properties of titanium diboride, J. Res. Natl. Inst. Stand. Technol. 105 (2000) 709, https://doi.org/10.6028/jres.105.057.
[43] B. Basu, G.B. Raju, A.K. Suri, Processing and properties of monolithic TiB 2 based materials, Int. Mater. Rev. 51 (2006) 352–374, https://doi.org/10.1179/174328006X102529.
[44] Z. Ahmadi, B. Nayebi, M. Shahedi Asl, I. Farahbakhsh, Z. Balak, Densification improvement of spark plasma sintered TiB2-based composites with micron-, submicron- and nano-sized SiC particulates, Ceram. Int. 44 (2018) 11431–11437, https://doi.org/10.1016/j.ceramint.2018.03.202.
[45] A. Sabahi Namini, S.A.A. Dilawary, A. Motallebzadeh, M. Shahedi Asl, Effect of TiB2 addition on the elevated temperature tribological behavior of spark plasma sintered Ti matrix composite, Compos. B Eng. 172 (2019) 271–280, https://doi.org/10.1016/j.compositesb.2019.05.073.
[46] K. Farhadi, A. Sabahi Namini, M. Shahedi Asl, A. Mohammadzadeh, M. Ghassemi Kakroudi, Characterization of hot pressed SiC whisker reinforced TiB2 based composites, Int. J. Refract. Metals Hard Mater. 61 (2016) 84–90, https://doi.org/10.1016/j.ijrmhm.2016.08.004.
[47] A. Sabahi Namini, M. Azadbeh, M. Shahedi Asl, Effects of in-situ formed TiB whiskers on microstructure and mechanical properties of spark plasma sintered Ti–B4C and Ti–TiB2 composites, Sci. Iran. 25 (2018) 762–771, https://doi.org/10.24200/sci.2017.4499.
[48] M. Vajdi, F. Sadegh Moghanlou, Z. Ahmadi, A. Motallebzadeh, M. Shahedi Asl, Thermal diffusivity and microstructure of spark plasma sintered TiB2-SiC-Ti composite, Ceram. Int. 45 (2019) 8333–8344, https://doi.org/10.1016/j.ceramint.2019.01.141.
[49] A. Sabahi Namini, A. Motallebzadeh, B. Nayebi, M. Shahedi Asl, M. Azadbeh, Microstructure–mechanical properties correlation in spark plasma sintered Ti–4.8 wt.% TiB2 composites, Mater. Chem. Phys. 223 (2019) 789–796, https://doi.org/10.1016/j.matchemphys.2018.11.057.
[50] M. Dashti Germi, Z. Hamidzadeh Mahaseni, Z. Ahmadi, M. Shahedi Asl, Phase evolution during spark plasma sintering of novel Si3N4-doped TiB2–SiC composite, Mater. Char. 145 (2018) 225–232, https://doi.org/10.1016/j.matchar.2018.08.043.
[51] F. Shayesteh, S.A. Delbari, Z. Ahmadi, M. Shokouhimehr, M. Shahedi Asl, Influence of TiN dopant on microstructure of TiB2 ceramic sintered by spark plasma, Ceram. Int. (2018), https://doi.org/10.1016/j.ceramint.2018.11.228.
[52] F. Sadegh Moghanlou, M. Vajdi, J. Sha, A. Motallebzadeh, M. Shokouhimehr, M. Shahedi Asl, A numerical approach to the heat transfer in monolithic and SiC reinforced HfB2, ZrB2 and TiB2 ceramic cutting tools, Ceram. Int. (2019), https://doi.org/10.1016/j.ceramint.2019.05.095.
[53] R. Königshofer, S. Fürnsinn, P. Steinkellner, W. Lengauer, R. Haas, K. Rabitsch, M. Scheerer, Solid-state properties of hot-pressed TiB2 ceramics, Int. J. Refract. Metals Hard Mater. 23 (2005) 350–357, https://doi.org/10.1016/j.ijrmhm.2005.05.006.
[54] S.A. Delbari, B. Nayebi, E. Ghasali, M. Shokouhimehr, M. Shahedi Asl, Spark plasma sintering of TiN ceramics codoped with SiC and CNT, Ceram. Int. 45 (2019) 3207–3216, https://doi.org/10.1016/j.ceramint.2018.10.223.
[55] M. Shahedi Asl, A. Sabahi Namini, M. Ghassemi Kakroudi, Influence of silicon carbide addition on the microstructural development of hot pressed zirconium and titanium diborides, Ceram. Int. 42 (2016) 5375–5381, https://doi.org/10.1016/j.ceramint.2015.12.072.
[56] Z. Hamidzadeh Mahaseni, M. Dashti Germi, Z. Ahmadi, M. Shahedi Asl, Microstructural investigation of spark plasma sintered TiB2 ceramics with Si3N4 addition, Ceram. Int. 44 (2018) 13367–13372, https://doi.org/10.1016/j.ceramint.2018.04.171.
[57] A. Sabahi Namini, M. Azadbeh, M. Shahedi Asl, Effect of TiB2 content on the characteristics of spark plasma sintered Ti–TiBw composites, Adv. Powder Technol. 28 (2017) 1564–1572, https://doi.org/10.1016/j.apt.2017.03.028.
[58] M. Shahedi Asl, Z. Ahmadi, S. Parvizi, Z. Balak, I. Farahbakhsh, Contribution of SiC particle size and spark plasma sintering conditions on grain growth and hardness of TiB2 composites, Ceram. Int. 43 (2017) 13924–13931, https://doi.org/10.1016/j.ceramint.2017.07.121.
[59] Y. Orooji, E. Ghasali, M. Moradi, M.R. Derakhshandeh, M. Alizadeh, M. Shahedi Asl, T. Ebadzadeh, Preparation of mullite-TiB2-CNTs hybrid composite through spark plasma sintering, Ceram. Int. (2019), https://doi.org/10.1016/j.ceramint.2019.05.154.
[60] M. Shahedi Asl, S.A. Delbari, F. Shayesteh, Z. Ahmadi, A. Motallebzadeh, Reactive spark plasma sintering of TiB2–SiC–TiN novel composite, Int. J. Refract. Metals Hard Mater. 81 (2019) 119–126, https://doi.org/10.1016/j.ijrmhm.2019.02.022.
[61] A. Sabahi Namini, S.N. Seyed Gogani, M. Shahedi Asl, K. Farhadi, M. Ghassemi Kakroudi, A. Mohammadzadeh, Microstructural development and mechanical properties of hot pressed SiC reinforced TiB2 based composite, Int. J. Refract. Metals Hard Mater. 51 (2015) 169–179, https://doi.org/10.1016/j.ijrmhm.2015.03.014.
[62] S. Nekahi, F. Sadegh Moghanlou, M. Vajdi, Z. Ahmadi, A. Motallebzadeh, M. Shahedi Asl, Microstructural, thermal and mechanical characterization of TiB2–SiC composites doped with short carbon fibers, Int. J. Refract. Metals Hard Mater. 82 (2019) 129–135, https://doi.org/10.1016/j.ijrmhm.2019.04.005.
[63] J. Zou, J. Liu, G.-J. Zhang, S. Huang, J. Vleugels, O. Van der Biest, J.Z. Shen, Hexagonal BN-encapsulated ZrB2 particle by nitride boronizing, Acta Mater. 72 (2014) 167–177, https://doi.org/10.1016/j.actamat.2014.03.054.
[64] J. Zou, G.-J. Zhang, C.-F. Hu, T. Nishimura, Y. Sakka, H. Tanaka, J. Vleugels, O. Van der Biest, High-temperature bending strength, internal friction and stiffness of ZrB2–20vol% SiC ceramics, J. Eur. Ceram. Soc. 32 (2012) 2519–2527, https://doi.org/10.1016/j.jeurceramsoc.2012.01.035.
[65] NASA, Power Turbine, Glenn Research Center (n.d), www.grc.nasa.gov/WWW/K-12/airplane/powturb.html.
[66] F. Nakamori, Y. Ohishi, H. Muta, K. Kurosaki, K. Fukumoto, S. Yamanaka, Mechanical and thermal properties of bulk ZrB2, J. Nucl. Mater. 467 (2015) 612–617, https://doi.org/10.1016/j.jnucmat.2015.10.024.
[67] J.B. Wachtman, W.E. Tefft, D.G. Lam, C.S. Apstein, Exponential temperature dependence of Young's modulus for several oxides, Phys. Rev. 122 (1961) 1754–1759, https://doi.org/10.1103/PhysRev.122.1754.
[68] V.V. Skripnyak, V.A. Skripnyak, Predicting the mechanical properties of ultra-high temperature ceramics, Lett. Mater. 7 (2017) 407–411, https://doi.org/10.22226/2410-3535-2017-4-407-411.
[69] N.L. Okamoto, M. Kusakari, K. Tanaka, H. Inui, S. Otani, Anisotropic elastic constants and thermal expansivities in monocrystal CrB2, TiB2, and ZrB2, Acta Mater. 58 (2010) 76–84, https://doi.org/10.1016/j.actamat.2009.08.058.
[70] P. Dahlander, Source Term Model Approaches to Film Cooling Simulations, Chalmers University of Technology, 2001.
[71] J. Bredberg, Turbulence Modelling for Internal Cooling of Gas-Turbine Blades, Chalmers University of Technology, Göteborg, Sweden, 2002.
[72] M. yaghoub Abdollahzadeh Jamalabadi, Thermal radiation effects on creep behavior of the turbine blade, Multidiscip. Model. Mater. Struct. 12 (2016) 291–314, https://doi.org/10.1108/MMMS-09-2015-0053.
[73] M. Patel, V.V.B. Prasad, V. Jayaram, Heat conduction mechanisms in hot pressed ZrB2 and ZrB2–SiC composites, J. Eur. Ceram. Soc. 33 (2013) 1615–1624, https://doi.org/10.1016/j.jeurceramsoc.2013.03.006.